

# Optimizing co-operative multi-environment dynamics in a dark-state-enhanced photosynthetic heat engine

Melina Wertnik,<sup>1,2</sup> Alex Chin,<sup>3</sup> Franco Nori,<sup>1,4</sup> and Neill Lambert<sup>1,a)</sup>

<sup>1</sup>Theoretical Quantum Physics Laboratory, RIKEN Cluster for Pioneering Research, Wako-shi, Saitama 351-0198, Japan

<sup>2</sup>Theoretical Physics, ETH Zurich, CH-8093 Zurich, Switzerland

<sup>3</sup>Institut des NanoSciences de Paris, Sorbonne Université, 4 Place Jussieu, Bote Courrier 840, 75252 Paris Cedex 05, France

<sup>4</sup>Department of Physics, University of Michigan, Ann Arbor, Michigan 48109-1040, USA

(Received 22 May 2018; accepted 9 August 2018; published online 30 August 2018)

We analyze the role of coherent, non-perturbative system-bath interactions in a photosynthetic heat engine. Using the reaction-coordinate formalism to describe the vibrational phonon-environment in the engine, we analyze the efficiency around an optimal parameter regime predicted in earlier studies. We show that, in the limit of high-temperature photon irradiation, the phonon-assisted population transfer between bright and dark states is suppressed due to dephasing from the photon environment, even in the Markov limit where we expect the influence of each bath to have an independent and additive effect on the dynamics. Manipulating the phonon bath properties via its spectral density enables us to identify both optimal low- and high-frequency regimes where the suppression can be removed. This suppression of transfer and its removal suggests that it is important to consider carefully the non-perturbative and cooperative effects of system-bath environments in designing artificial photosynthetic systems and also that manipulating inter-environmental interactions could provide a new multidimensional “lever” by which photocells and other types of quantum devices can be optimized. *Published by AIP Publishing.* <https://doi.org/10.1063/1.5040898>

## I. INTRODUCTION

The observation of what might be quantum coherent beating over time scales comparable to energy transfer in a range of photosynthetic light-harvesting complexes<sup>1–7</sup> has, while still open to interpretation, inspired efforts to identify mechanisms by which coherence can in principle increase the efficiency of energy harvesting, even if nature itself does not do so. For example, it has been proposed that the combination of noise<sup>8–15</sup> and quantum tunnelling (collectively called “environment assisted quantum tunneling”) can in principle assist energy transfer on its way,<sup>16,17</sup> allowing it to overcome energetic barriers to transport.<sup>1,3,6,7,18,19</sup>

Recently, another mechanism<sup>20–22</sup> was proposed, in the context of recasting the standard model of a light-absorbing photosynthetic reaction center as a “quantum heat engine.” The idea of recasting light-harvesting in terms of a heat-engine was arguably originally presented by Shockley and Quisser,<sup>23</sup> who derived the efficiency of inorganic photovoltaics using thermodynamic arguments. More recently, Dorfman *et al.*<sup>20</sup> generalized this idea with the goal of analyzing small molecular systems with similar thermodynamic arguments. In this context, a “quantum heat engine” can be thought of as the ultimate limit of a classical heat engine, in that it describes the movement of a single excitation through a series of processes such that some of the input energy can be used for

a useful purpose. The ultimate goal of these approaches is both to understand naturally existing systems and to identify clear mechanisms which enhance efficiencies of such “quantum light harvesting heat engines,” which may eventually be applicable to artificial photosynthetic systems and photocells.<sup>7,24</sup>

In the examples studied in Refs. 20–22, they were able to identify a new “coherence” mechanism that improved efficiency. In the example presented in those studies, the collective dipole coupling of two chromophores to incident light leads to interference effects that create “bright” and “dark” states. Other mechanisms, such as direct coupling<sup>21</sup> or environment-induced interference effects,<sup>20,25</sup> can then lead to the energetic splitting of these states and subsequent breaking of detailed balance<sup>26</sup> for the photon absorption process. The suppression of spontaneous and stimulated emission of photons leads to an overall increased efficiency and can be thought of as a way to overcome the Shockley limit on absorption.<sup>23</sup>

The nature of the coherent and non-perturbative interaction between the dimer and its phonon environment has further potential to enhance the efficiency.<sup>27–36</sup> This is particularly appealing when such problems are recast as “quantum heat engines,” as it allows us to view the problem of improving efficiency through the lens of non-Markovian thermodynamics and understand this phonon environment as a “cold bath,” whose properties can be manipulated and taken advantage of to maximise energy extraction from a “hot” environment.<sup>32</sup>

<sup>a)</sup>E-mail: [nwlambert@gmail.com](mailto:nwlambert@gmail.com)

In this work, we investigate how to modify the phonon environment to optimize the efficiency of such a light-harvesting “quantum heat engine,” as realized by two coupled chromophores.<sup>20–22</sup> To describe the complex problem of chromophores strongly interacting with their phonon (or vibronic) environment, which plays the role of the cold-bath in the heat engine picture, many techniques of varying degrees of sophistication and approximation have been developed. These, among many,<sup>37</sup> include perturbative but non-Markovian methods<sup>38,39</sup> and exact methods, like the “hierarchy equations of motion,”<sup>2,40,41</sup> the reaction-coordinate (RC) method,<sup>32,35,42–44</sup> and the quasi-adiabatic path-integral<sup>45,46</sup> approach. For zero temperature simulations, powerful, numerically exact many-body methods are also available, such as the multiconfigurational time-dependent Hartree Fock and tensor network approaches which give access to the dynamics of both the system and environment.<sup>47–51</sup>

The reaction-coordinate (RC) method, which we employ herein, has been proposed as a particularly powerful tool for these types of problems. It allows for a straightforward evaluation of thermodynamic quantities,<sup>32,35</sup> can be applied selectively to a many-bath system (in concert with normal Markovian methods to describe other baths), and can describe both low and high-frequency baths for arbitrary coupling strengths.<sup>52</sup>

### A. Summary of results

Here we show, using this reaction coordinate method, that in the high-temperature photon irradiation limit, and fast donor-acceptor transfer, which in the classical case both optimizes the Carnot efficiency and leads to a large current, the interaction between the chromophores and the phonon environment is dephased to such a degree that the photo-induced current is suppressed. This result is an explicit example of how the interplay of multiple environments can be non-additive and lead to unexpected results.<sup>51,53–55</sup> Indeed, the importance of such effects extends beyond the case of light-harvesting to a wider range of nanoscale devices strongly coupled to multiple environments, such as in lead-dot(molecule)-lead structures.<sup>56</sup> We show how this suppression can be overcome by increasing the coupling to the phonon environment such that it is more strongly influencing the chromophore system than an equivalent Markovian environment.

The assumption of high-photon irradiation temperature<sup>20–22,30,34</sup> does not occur with natural sunlight. Thus, we also examine, in Sec. IV B, the low-temperature photon irradiation case, with parameters corresponding to more realistic, but optimally concentrated, natural sunlight irradiation. Here we find that in the Born-Markov limit of the phonon environment, the baths again become additive. We also show that entering into the non-Markovian and strong-coupling limit for this bath ultimately has diminishing returns in this low-temperature case. The mechanism of this diminishment is shown, via perturbation theory, to arise from the “counter-rotating” terms in the interaction with the phonons, which reduce the relative populations of the donor states which couple to the acceptor.

The overall structure of this work is as follows. We begin by defining our heat engine model in Sec. II. We then describe

the reaction-coordinate method for modeling the phonon environment in Sec. III. In Sec. IV, we discuss the results of our model, and explore both high and low photon temperature regimes, and give our conclusions in Sec. V. In the Appendix, we define the secular and non-secular Markovian master equations to which we compare our results.

## II. MODEL: PHOTOSYNTHETIC QUANTUM HEAT ENGINE

A minimal model (cf. Fig. 1) of a photosynthetic quantum heat engine describes the excitonic states of three molecules: a pair of coupled donor molecules  $D_1$  and  $D_2$  and one acceptor molecule  $A$ . As discussed by Creatore *et al.*,<sup>21</sup> a dipole-dipole interaction leads to strong coupling between the two donor molecules, transforming the originally degenerate excited states  $|a_1\rangle$  and  $|a_2\rangle$  into new non-degenerate eigenstates  $|x_{1,2}\rangle = 1/\sqrt{2}(|a_1\rangle \pm |a_2\rangle)$  with eigenvalues  $E_{x_{1,2}} = E_{1,2} \pm J$ , where  $J$  is the coupling amplitude. Due to the collective way, the parallel dipole moments add up, and only  $|x_1\rangle$  is optically active.

Photon absorption (from a hot concentrated photon bath with thermal occupation  $n_h$ ) occurs at a rate  $\gamma_h$ , causing transitions from the unexcited state  $|b\rangle$  to the donor excited states  $|a_1\rangle$  and  $|a_2\rangle$ . Ultimately, the collective nature of that absorption leads to occupation of only the bright state  $|x_1\rangle$ , which then can relax to the dark state  $|x_2\rangle$  by emission of phonons into an environment with thermal occupation  $n_x$ . In the Markovian model, this exchange is described by a rate  $\gamma_x$ , whereas

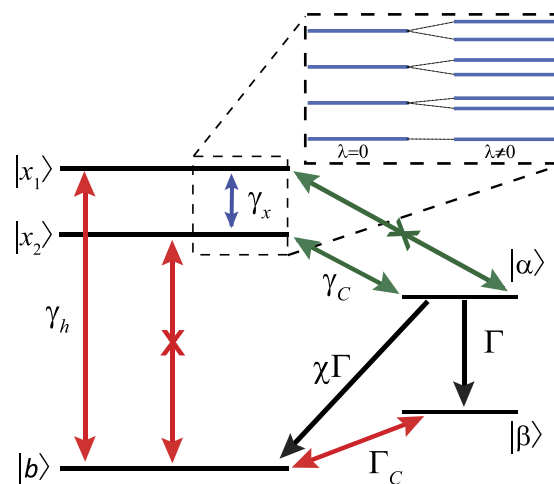


FIG. 1. Scheme for the five level model<sup>21</sup> in the coupled basis. A photon excites the donor molecules from the collective ground state  $|b\rangle$  to the collective bright excited state  $|x_1\rangle$ . This excitation is then transferred, via energy exchange with the phonon bath, to the dark state  $|x_2\rangle$ . Work can then be extracted via a charge transfer process to  $|\alpha\rangle$  and  $|\beta\rangle$  before the system is reset to the collective ground state. The red transition ( $\gamma_h$ ) stems from absorption and emission of photons, the transitions due to transfer of electrons between donors and acceptors ( $\gamma_c$ ,  $\Gamma_c$ ) are rendered in green, while the transitions in black ( $\Gamma$ ,  $\chi\Gamma$ ) model the extraction of work as well as the recombination loss from  $|\alpha\rangle$  to the ground state. With the Reaction Coordinate (RC) method, the transition between the two donor excited states (given by a rate  $\gamma_x$  in the Born-Markov model<sup>21</sup>) is treated non-perturbatively by coupling the system to a collective degree of freedom in the phonon bath with coupling strength  $\lambda_0$ . The inset shows the lowest lying energy levels of the  $x_1$  and  $x_2$  states coupled to the collective RC mode for a coupling strength of  $\lambda_0 = 1.06 \times 10^{-3} \text{ eV}^{3/2}$  at the resonant frequency  $\Omega_0 = 0.03 \text{ eV}$  [cf. Fig. 2(a)].

in the RC model, which we describe in Sec. III, the interaction with a collective mode is used. Occupation of the dark state breaks detailed balance, allowing time for an electron to be transferred to the acceptor molecule, taking the system to the acceptor excited state  $|\alpha\rangle$  (at a bare rate  $\gamma_c$ , assisted by a thermal environment with occupation  $n_c$ ).

This charge transfer is suppressed for the bright state due to the electron transfer matrix elements carrying opposing signs,  $t_{D_1,A} = -t_{D_2,A}$ . At  $|\alpha\rangle$ , work is extracted, leading the system to the ground state of the acceptor molecule  $|\beta\rangle$ , at rate  $\Gamma$ . Additionally, an effective lossy transition to the donor ground state is described by the rate  $\chi\Gamma$ , which represents additional losses by which the system is reset without producing work. Finally, after work has been extracted,  $\Gamma_c$  describes the other “reset” process of the system back to the ground state  $|b\rangle$ , e.g., due to donation of a charge to the original donor molecule from the environment.<sup>57</sup> In our model, this transition is assisted by a different thermal environment with occupation  $N_c$ . Note that all the transition rates involving the donor excited states are twice as large in the coupled basis than they are in the uncoupled basis.

The role of the phonon environment in transferring population must be considered carefully. In real, photosynthetic systems such environments typically exist in the non-perturbative and non-Markovian regimes, with both bath correlation times and system-bath correlation times being of the same order as excitonic couplings (the parameter  $J$  in our model). Indeed, understanding the open system physics of this “intermediate regime,” where system and bath must be treated on the same footing, is the principle motivation for the diversity of powerful open system techniques mentioned in the introduction.

The Hamiltonian describing the two donors, the acceptor molecule, and the phonon environment is

$$H = H_S + H_B + H_I, \quad (1)$$

$$H_S = \sum_{i=1}^5 \mathcal{E}_i |\psi_i\rangle\langle\psi_i| + J(|a_2\rangle\langle a_1| + |a_1\rangle\langle a_2|),$$

$$H_B + H_I = \frac{1}{2} \sum_k \left[ p_k^2 + \omega_k^2 \left( x_k - \frac{f_k}{\omega_k^2} s \right)^2 \right],$$

with mass-weighted positions  $x_k = 1/\sqrt{2\omega_k}(c_k^\dagger + c_k)$  and momenta  $p_k = i\sqrt{\omega_k/2}(c_k^\dagger - c_k)$  of the bath fulfilling  $[x_k, p_l] = i\delta_{kl}$  (setting  $\hbar \equiv 1$  throughout) and with creation and annihilation operators  $c_k^\dagger$  and  $c_k$ . The operator coupling

system and bath are given by

$$s = (|a_1\rangle\langle a_1| - |a_2\rangle\langle a_2|), \quad (2)$$

while the system is defined with the five states of the uncoupled molecules,

$$|\psi_i\rangle = \{|b\rangle, |a_1\rangle, |a_2\rangle, |\alpha\rangle, |\beta\rangle\}, \quad (3)$$

and corresponding energies  $\mathcal{E}_i = \{E_b, E_1, E_2, E_\alpha, E_\beta\}$ . As explained earlier, diagonalizing the system part of the Hamiltonian (when  $E_1 = E_2$ ) leads to two new eigenstates  $|x_{1,2}\rangle = 1/\sqrt{2}(|a_1\rangle \pm |a_2\rangle)$  with eigenvalues  $E_{x_{1,2}} = E_{1,2} \pm J$ . Also, not shown here are the explicit Hamiltonians for the other baths shown in Fig. 1. Their influence on the model will be defined explicitly later within the master equation picture.

### III. METHODS: THE REACTION COORDINATE

The dark-state-enhanced heat engine, including the dipole coupling  $J$ , has previously been studied<sup>21</sup> using a Born-Markov master equation description of the phonon bath [see Eq. (A1) in the Appendix] and has been compared to a model where the donors do not couple to each other. That work<sup>21</sup> found a relative current enhancement of the coupled ( $J > 0$ ) over the uncoupled ( $J = 0$ ) case of roughly 30%. To give a like-for-like comparison, we primarily use the parameters found in Ref. 21 that gave this large current enhancement in our simulations (cf. Table I), which focus on the limit of high photon irradiation. In Sec. IV B, we will consider the low-temperature photon case, which is more applicable to systems irradiated by natural sunlight.

Instead of employing a Born-Markov master equation, we construct a more general master equation that can take into account non-Markovian effects of the phonon environment. We do so using the reaction coordinate (RC) mapping<sup>42,58</sup> to transform the bath Hamiltonian such that a collective degree of freedom of the said environment is included in the “system” Hamiltonian, while the residual environment is treated with a traditional generalized master equation. The validity of this approach was carefully analyzed in Ref. 43 and, by comparison to the hierarchy method, found to be exact. It has been found to be particularly convenient for describing both under and over-damped Brownian motion spectral densities<sup>44</sup> and can, in principle, be extended to deal with more complex spectral densities.<sup>59</sup> However, if the original spectral density is very broad, the residual environment may also be effectively strongly coupled to the system, and in some cases

TABLE I. Parameters used for the numerical simulation.

Donor excitation energy	$\Delta_h = E_1 - E_b = E_2 - E_b$	1.8 eV
Donor-acceptor energy difference	$\Delta_c = E_1 - E_\alpha = E_2 - E_\alpha = E_\beta - E_b$	0.2 eV
Excitonic coupling	$J$	0.015 eV
Photon absorption rate	$\gamma_h$	$6.2 \times 10^{-7}$ eV
Donor-acceptor charge transfer rate	$\gamma_c$	$6 \times 10^{-3}$ eV (in Sec. IV), $1 \times 10^{-6}$ eV (in Sec. IV B)
Work extraction rate	$\Gamma$	0.124 eV
Reset rate	$\Gamma_c$	0.0248 eV
Photon occupation	$n_h$	$\sim 60\,000$ (in Sec. IV), $\sim 0.03$ (in Sec. IV B)
Charge transfer bath occupation	$N_c = n_c$ at 300 K	$\sim 4.4 \times 10^{-4}$
Phonon bath occupation (for the Born-Markov model)	$n_x$ at 300 K	$\sim 0.46$

a master equation approximation may break down. Here we do not benchmark the results against another technique, as in those earlier studies, and thus do not claim that our treatment of the phonon environment is exact to all orders for all parameter regimes we study herein. Rather, we propose that it captures more salient features than obtainable with a standard Born-Markov method alone.

### A. The reaction coordinate transformation

We follow the description of the RC method in Ref. 32 and repeat only the main steps here. Starting from the complete Hamiltonian [Eq. (1)], a transformation has to be found that maps the interaction of the phonon bath with the system onto one new coordinate (the RC). This reaction coordinate is itself coupled to a residual bath, which will be treated using the standard Born-Markov approximation. However, later we will see that relaxation rates induced by the residual phonon bath, as well as the hot photon bath and the donor-acceptor transfer process, can be of the order of the system frequencies such that we cannot make the secular approximation in describing these baths.<sup>60</sup> Therefore, we work with Born-Markov non-secular master equations for these particular environments.

Under this transformation, the system can be coupled arbitrarily strongly to the RC, as this is treated exactly through the  $H'_{RC}$  part of the transformed Hamiltonian

$$\begin{aligned} H' &= H'_S + H'_B + H'_I, \\ H'_S &= H_S + H_{RC}, \\ H_{RC} &= \frac{1}{2} \left[ P_1^2 + \frac{g_0^2}{\delta\Omega_0^2} \left( X_1 - \frac{\delta\Omega_0^2}{g_0} s \right)^2 \right], \\ H'_B + H'_I &= \frac{1}{2} \sum_k \left[ P_k^2 + \Omega_k^2 \left( X_k - \frac{C_k}{\Omega_k^2} X_1 \right)^2 \right]. \end{aligned} \quad (4)$$

Here  $g_0$  is the coupling strength between the reaction coordinate and the system, while  $X_1$  describes the collective quadrature of the RC mode. In this new frame, we treat the residual baths and their interaction with the system via the RC mode ( $H'_B + H'_I$ ) with the non-secular Born Markov master equation. The renormalization term  $\delta\Omega_0^2 s^2/2$  can be neglected as it is small compared to the energy difference between the excited states of the dimer and the states  $|b\rangle$  and  $|\alpha\rangle$ .

The details of the transformation of the Hamiltonian above are entirely defined by the choice of spectral density for the *original* phonon environment,

$$J_0(\omega) \equiv \frac{\pi}{2} \sum_k \frac{f_k^2}{\omega_k} \delta(\omega - \omega_k). \quad (5)$$

Here we focus on the underdamped Brownian oscillator spectral density,

$$J_0(\omega) = \frac{\lambda_0^2 \gamma \omega}{(\omega^2 - \Omega_0^2)^2 + \gamma^2 \omega^2}, \quad (6)$$

as it allows us to investigate the influence of resonant and off-resonant structured environments that can dominate the vibrational spectrum of light-harvesting complexes.<sup>61</sup>

The choice<sup>32</sup> of spectral density ultimately fixes the coupling strength  $g_0$  and the RC frequency  $\frac{g_0}{\delta\Omega_0}$ . From the transformation of the Hamiltonian, we obtain a term for the coupling strength as well as for the system renormalization,

$$\begin{aligned} g_0^2 &= \sum_k f_k^2, \\ \delta\Omega_0^2 &= \sum_k \frac{f_k^2}{\omega_k^2}. \end{aligned} \quad (7)$$

These can then be expressed through integrals over the spectral density  $J_0(\omega)$  and evaluated as

$$\begin{aligned} g_0^2 &= \frac{2}{\pi} \int_0^\infty d\omega J_0(\omega) \omega = \lambda_0^2, \\ \delta\Omega_0^2 &= \frac{2}{\pi} \int_0^\infty d\omega \frac{J_0(\omega)}{\omega} = \frac{\lambda_0^2}{\Omega_0^2}. \end{aligned} \quad (8)$$

The physical frequency of the RC is given by  $\frac{g_0}{\delta\Omega_0} = \Omega_0$ , hence  $X_1 = (a + a^\dagger)/\sqrt{2\Omega_0}$ , and we can now identify the coupling strength  $g_0 = \lambda_0$ .

The spectral density of the residual bath is connected to the original environment through a recursion relation.<sup>59</sup> By deriving the Fourier space propagator from the original and transformed Hamiltonian and comparing them,<sup>32</sup> the transformed spectral density can be found by evaluating

$$J_1(\omega) = \frac{\lambda_0^2 J_0(\omega)}{|W_0^+(\omega)|^2}, \quad (9)$$

where

$$W_0^+(z) = \lim_{\epsilon \rightarrow 0^+} \frac{1}{\pi} \int_{-\infty}^\infty d\omega \frac{J_0(\omega)}{\omega - (z + i\epsilon)} \quad (10)$$

is the Cauchy transform of the original spectral density  $J_0$ . Using the residue theorem, our choice of the original spectral density [Eq. (6)] leads to an Ohmic spectral density for the residual bath,  $J_1(\omega) = \gamma\omega$ .

### B. Master equation approximations

We are mainly interested in the steady-state current output for various input parameters, which is calculated numerically from the steady-state density matrix  $\rho(t \rightarrow \infty)$ .<sup>62,63</sup> The master equation used to solve for  $\rho(t \rightarrow \infty)$  is split into three parts:

1. The transition between the donor excited states,  $|x_1\rangle$  and  $|x_2\rangle$ , due to the interaction with the phonon environment, is treated by the system and RC parts of the Hamiltonian  $H'_S$ .
2. The residual baths coupled to the RC mode, as well as the transitions involving the donor excited states, are described by a non-secular Born-Markov master equation.
3. The transitions not involving the donor excited and RC states are treated using phenomenological secular Born-Markov Lindblad generators.

We cannot use the secular approximation in point 2 because to do so, the time scales of the system have to be much smaller than the relaxation times:  $\tau_S \ll \tau_R$ . The system time scale is proportional to the inverse of the energy splitting, while the relaxation time is defined through the transition

rates and occupation numbers. The condition for the secular approximation to be valid then becomes

$$2J, \frac{\lambda_0}{\sqrt{2\Omega_0}} \gg (n_h + 1)\gamma_h, (1 + n_c)\gamma_c, (1 + n_x)\gamma. \quad (11)$$

Even without the RC-mode description of the phonon bath, this condition is not fully satisfied because the rate of absorption and emission of photons,  $(n_h + 1)\gamma_h$ , is comparable to  $2J$ . However, by introducing the RC, the energy splittings in the system Hamiltonian become even smaller (cf. Fig. 1) such that a non-secular approach is necessary for both the photon bath as well as the electron transfer.

Our general master equation, including generators for both secular ( $\mathcal{L}$ ) and non-secular ( $\mathcal{M}$ ) baths, is

$$\begin{aligned} \dot{\rho}(t) = & -i[H'_S, \rho(t)] + \mathcal{M}_{X_1}[\rho(t)] + \mathcal{M}_{Q_h}[\rho(t)] \\ & + \mathcal{M}_{Q_c^{(\omega)}}[\rho(t)] + \mathcal{L}_{\beta b}[\rho(t)] + \mathcal{L}_{b\beta}[\rho(t)] \\ & + \mathcal{L}_{\alpha\beta}[\rho(t)] + \mathcal{L}_{\alpha b}[\rho(t)]. \end{aligned} \quad (12)$$

As described in item 2 above, for the baths which couple to the RC mode directly, or via the donor excited states, we use non-secular generators.<sup>64</sup> These generators take into account both the coupled eigenstructure of the donors and RC mode and the potentially highly dissipative nature of the baths. A full derivation of this type of the master equation in the context of the RC formalism can be found in Refs. 32 and 43, but here we just report their generic form,

$$\mathcal{M}_A[\rho(t)] = -[A, [\chi, \rho(t)]] + [A, \{\Theta, \rho(t)\}], \quad (13)$$

where the label  $A$  refers to the particular system operator which couples to the given environment and

$$\begin{aligned} \chi &= \frac{1}{2} \sum_{kl} J_A(\omega_{kl}) \coth\left(\frac{\beta_A \omega_{kl}}{2}\right) A_{kl} |k\rangle\langle l|, \\ \Theta &= \frac{1}{2} \sum_{kl} J_A(\omega_{kl}) A_{kl} |k\rangle\langle l|, \end{aligned} \quad (14)$$

where  $A_{kl} = \langle k|A|l\rangle$ , and the eigenvectors  $|k\rangle$  and eigenenergies  $\omega_{kl}$  are calculated from  $H'_S$  in Eq. (4). In addition,  $J_A(\omega)$  is the spectral density of said environment, and  $\beta_A = 1/k_B T_A$  is its inverse temperature.

For the residual bath coupled to the RC mode, the system operator is given by the RC mode operator  $X_1 = (a + a^\dagger)/\sqrt{2\Omega_0}$ , and the spectral density is given by  $J_{X_1}(\omega) = J_1(\omega) = \gamma\omega$ . For the transitions between  $|b\rangle$  and  $|x_1\rangle$ , and between  $|x_2\rangle$  and  $|\alpha\rangle$ , the transition operators

$$Q_h = (|a_1\rangle + |a_2\rangle)\langle b| + |b\rangle(\langle a_1| + \langle a_2|) \quad (15)$$

and

$$Q_c^{(\omega)} = |\alpha\rangle(\langle a_1| - \langle a_2|) + (|a_1\rangle - |a_2\rangle)\langle \alpha| \quad (16)$$

are used and the spectral density for these baths is assumed to be Ohmic,

$$J_{h,c}(\omega) = \frac{\gamma_{h,c}}{2\Delta_{h,c}} \omega, \quad (17)$$

for each of them, respectively: where the donor excitation energies are  $\Delta_h = E_1 - E_b = E_2 - E_b$ , and the donor-acceptor energy difference is  $\Delta_c = E_1 - E_\alpha$ , as per Table I. The residual phonon bath temperature and donor-acceptor transition rate temperature are set to 300 K, but the transition between the ground

state and  $|x_1\rangle$  is governed by the photon bath, defined through its occupation number given in Table I.

The environments which do not couple directly to the excited donor states, as described in item 3 above, are given by secular Born-Markov Lindblad generators

$$\mathcal{L}_{AB} = \left[ C_{AB} \rho(t) C_{AB}^\dagger - \frac{1}{2} \{ C_{AB}^\dagger C_{AB}, \rho(t) \} \right], \quad (18)$$

where the indices  $A$  and  $B$  now refer to the states between which the Lindblad operator causes transitions,

$$\begin{aligned} C_{\beta b} &= \sqrt{\Gamma_c N_c} |\beta\rangle\langle b|, \\ C_{b\beta} &= \sqrt{\Gamma_c (1 + N_c)} |b\rangle\langle \beta|, \\ C_{\alpha\beta} &= \sqrt{\Gamma} |\beta\rangle\langle \alpha|, \\ C_{\alpha b} &= \sqrt{\chi \Gamma} |b\rangle\langle \alpha|. \end{aligned} \quad (19)$$

For these baths, a Lindblad treatment is sufficient, as they are insensitive to the eigenstructure of the donors coupled to the RC mode. The two (secular and non-secular) Markovian master equations without the reaction coordinate, to which we compare our results, are given in the Appendix.

#### IV. RESULTS AND DISCUSSION

Here we will present and discuss the characteristics of the current generated by our RC method and compare them with the secular Born-Markov master equation model studied in Ref. 21, cf., Eq. (A1), as well as the non-secular equivalent, Eq. (A3), which takes into account that the transitions  $\gamma_h n_h$  and  $\gamma_c n_c$  can be of the order of the energy splitting  $2J$ . We define the current as proportional to the rate of population transfer from  $|\alpha\rangle$  to  $|\beta\rangle$ , i.e.,

$$j = e\Gamma \langle \alpha | \rho | \alpha \rangle. \quad (20)$$

We choose an effective transition rate for the influence of the phonon environment on the system such that  $\gamma_x \equiv 2J_0(\omega = 2J)$  which, after setting the resonance  $\Omega_0$  and width  $\gamma$ , determines  $\lambda_0$  in the RC model. For example, choosing  $\gamma_x = 25$  meV, and setting the spectral density to be resonant  $\Omega_0 = 2J$ , and choosing a narrow distribution,  $\gamma = 0.1\Omega_0$ ,  $\lambda_0 = \sqrt{J\gamma\gamma_x}$ , we find, surprisingly, that the current is roughly three times lower using the RC method than using either Born-Markov master equations (cf. Fig. 2).

Away from resonance, the relaxation rate  $\gamma_x$  decreases rapidly. As mentioned, the spectral density has been chosen such that the value for  $\omega = \Omega_0$  corresponds to the transition rate  $\gamma_x$ . Thus one would expect a maximal current at resonance, where the frequency of the phonon bath corresponds to the energy gap between states  $|x_1\rangle$  and  $|x_2\rangle$  and  $\gamma_x$  is maximal for constant coupling strength  $\lambda_0$ . If one increases the RC frequency above the resonance frequency, the current indeed decreases steadily toward zero, albeit this decay is much slower in the RC method than in the Born-Markov master equation.

##### A. Suppression of current

The counter-intuitive suppression of the current arises from the non-secular nature of the *photon* environment and is not captured by a standard secular master equation. Its origin

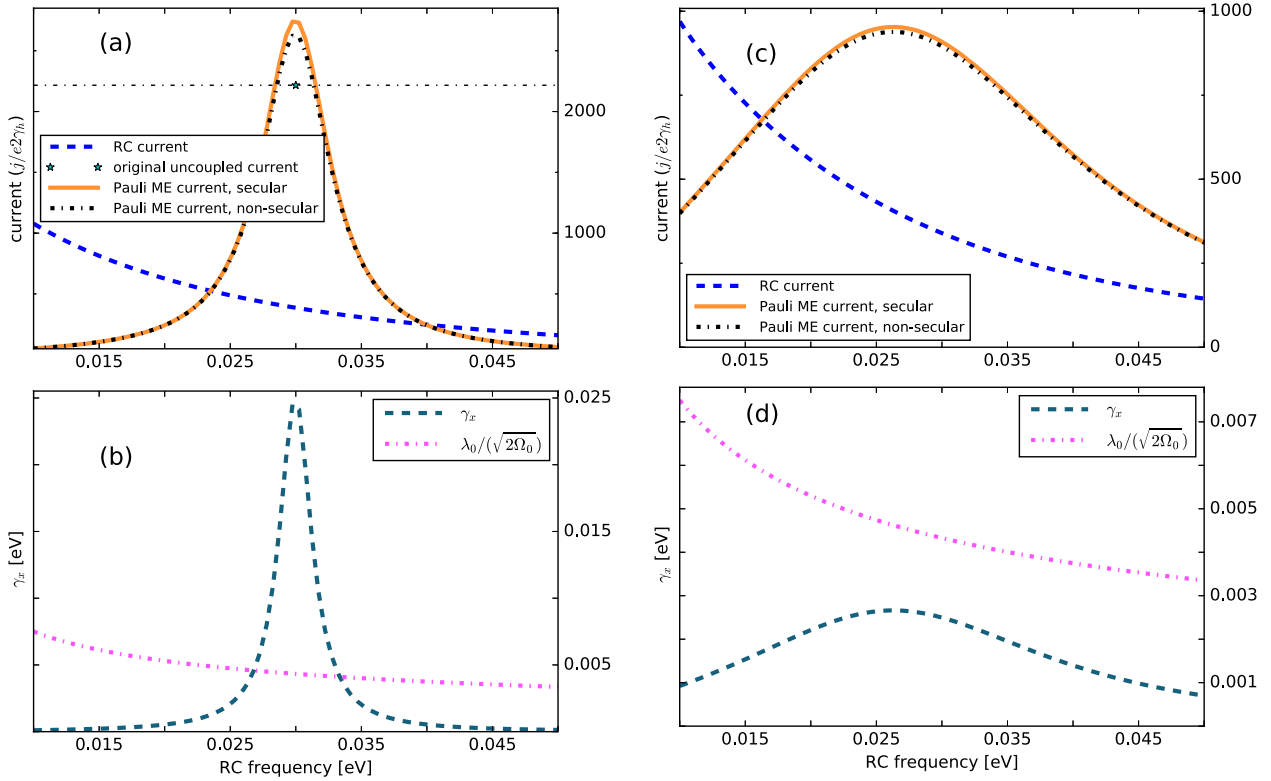


FIG. 2. Current as a function of the reaction coordinate (RC) frequency  $\Omega_0$  (eV) (i.e., the peak in the spectral density) for  $\lambda_0 = 1.06 \times 10^{-3} \text{ eV}^{3/2}$  and for different values of  $\gamma$ . This is compared to the current for a model without the RC-mode, which has been calculated using the equivalent Born-Markov master equation and is a function of the transition rate  $\gamma_x$  corresponding to the given RC frequency and coupling strength. (a)  $\gamma = 0.1\Omega_0$ : In this example, we use the default parameters shown in Table I and compare the current from the secular (orange curve) and non-secular Born-Markov ME (black dash-dotted curve) and the RC method (blue dashed curve). The magnitude of the RC current at resonance only reaches about 15% of the one from the Born-Markov ME. At lower frequencies, the RC model predicts an increase in the current, which surpasses the equivalent Born-Markov ME current. As a reference point, the blue star/horizontal dashed line is the value of the current for the uncoupled model,  $J = 0$ , also calculated using an equivalent Born-Markov master equation, but with no phonon bath at all. (b) shows, with a blue-dashed curve, the dependence of  $\gamma_x$  on the resonant frequency (RC frequency) of the phonon spectral density. The pink dashed-dotted curve shows the effective coupling strength  $g_0/\sqrt{2\Omega_0} = \lambda_0/\sqrt{2\Omega_0}$  between the system and RC mode. (c)  $\gamma = \Omega_0$ : Using the same coupling strength  $\lambda_0$  but changing the broadness parameter of the spectral density leads to a decreased transition rate  $\gamma_x$ ; thus, the current from the Born-Markov ME lowers and broadens in turn. In this case, the RC current remains mostly unchanged, as it follows the behavior of the effective coupling strength [shown in (d)] instead of the transition rate [also illustrated in (d)].

lies in the fact that the strong illumination leads to fast emission and absorption between  $|x_1\rangle$  and  $|b\rangle$  such that phonon-mediated coherence between  $|x_1\rangle$  and  $|x_2\rangle$  cannot be built fast enough. The interaction with the phonon bath is effectively dephased by the high temperature of the photon bath, and population transfer to the  $|x_2\rangle$  state cannot occur. In other words, the photon environment rapidly “measures” the population in  $|x_1\rangle$ , causing a quantum Zeno effect. This is akin to the suppression of lasing seen in single-atom lasers at high inversion rates.<sup>65</sup> A minimal condition for this “Zeno” effect is

$$\gamma_h n_h, \gamma_c \gg \frac{\lambda_0}{\sqrt{2\Omega_0}}. \quad (21)$$

Using a non-Markovian bath under such strong illumination then seems, at first glance, counter-productive. Off-resonance, we can identify regions where the current exceeds that predicted by the equivalent Markovian master equation (cf. Fig. 2), but these remain smaller than those predicted by the uncoupled dimer model. In this parameter regime, the current from the RC model predominantly follows the change in the effective coupling strength  $\lambda_0/\sqrt{2\Omega_0}$ , increasing for lower RC frequencies and decreasing for higher ones,

due to the corresponding dependence of the maxima in the original spectral density. In addition, because we scale the width of the bath while changing the resonance frequency,  $\gamma \propto \Omega_0$ , at lower frequencies, the phonon environment is correspondingly more non-Markovian. Finally, the increased thermal occupation of a low-frequency RC mode also affects the increase in the current. By removing all three dependencies (rescaling the effective coupling strength, making  $\gamma$  constant, and lowering the temperature of the phonon bath), the dependence of the current on the RC frequency flattens out (cf. Fig. 3).

More generally, one expects that the current should be restored if the coupling to the phonon-environment is made competitive with the influence of dephasing, per Eq. (21). In Fig. 6(b), we can see that increasing the coupling strength between system and RC when they are resonant can increase the current, overcoming this suppression, but this current is still less than that predicted by the Born-Markov master equation, though it can exceed the uncoupled dimer model for exceedingly strong coupling. To find a regime where the RC model exceeds the Born-Markov master equations and the uncoupled dimer model, we simultaneously vary both RC frequency  $\Omega_0$

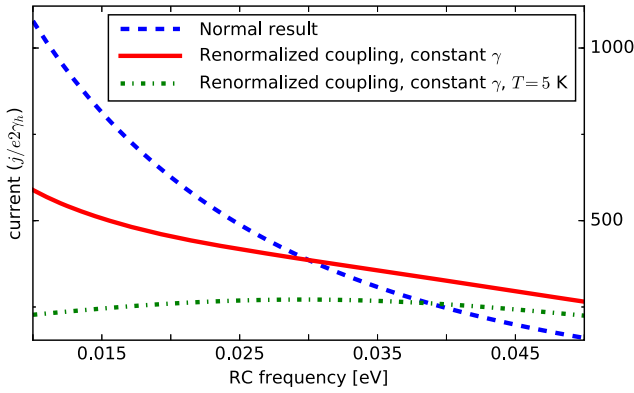


FIG. 3. A comparison of the current from the full RC model for three different conditions. The blue dashed curve shows the same result as in Fig. 2(a). The red solid curve shows the current when the effective coupling to the RC mode has been made independent of  $\Omega_0$  by rescaling  $\lambda_0 \rightarrow \sqrt{2\Omega_0}\lambda_0$  (which incidentally changes the units of  $\lambda_0$ ). In this curve, we also make  $\gamma$  a constant,  $\gamma = 0.2J$ , corresponding to its value at the resonance point in Fig. 2(a). Finally, the green dash-dotted curve is for the same changes with an additional reduction of the phonon temperature to  $T = 5$  K. This combination of alterations shows that the monotonically increasing current as  $\Omega_0 \rightarrow 0$  in Fig. 2(a) arises because of the dependence of the effective coupling strength on  $\Omega_0$  and the higher thermal occupation of the RC mode at low frequencies.

and coupling strength  $\lambda_0$  to keep the effective rate that the system sees in the Markovian model  $\gamma_x \equiv 2J_0(\omega = 2J) = 25$  meV fixed. In this case, we find a pronounced minimum around the resonant RC frequency (cf. Fig. 4), again because of the Zeno-like effect seen in Fig. 2. Under these constraints, for both lower and higher frequencies, the effective coupling strength increases away from resonance and so does the current, as the energy splittings due to interaction with the phonons exceed the suppressive dephasing rates.

In particular, one can immediately note that a very narrow spectral density ( $\gamma = 0.01\Omega_0$ ) can lead to a substantial current off-resonance. At very high frequencies (not explicitly shown in the figure), this can exceed the current predicted by the Born-Markov master equation for this optimal rate. This suggests that there are regimes where a structured environment can enhance the current. However, further optimizing this current, beyond the range shown in the figure, requires us to enter a regime that exceeds the limits of our numerical RC method and may be more amenable to methods used in other studies.<sup>34,36</sup> In addition, it should be noted that, as we tune far off resonance in Fig. 4, for the very narrow bath  $\gamma = 0.01\Omega_0$ , numerical convergence in the phonon Fock space becomes difficult, and the observed current should only be considered as a lower bound.

The dependence on the width of the spectral density in Fig. 4 also illustrates that while a sharper spectral density suppresses the current at resonance almost completely, and allows for a large current when off-resonance, a broader spectral density, with a correspondingly stronger coupling on resonance (to maintain the same  $\gamma_x$  effective rate), results in a larger current on resonance (albeit one still below that predicted by the Markov theory). When the same parameter  $\gamma$  is changed, but the coupling strength is kept constant [cf. Fig. 2(c)], the RC current does not change significantly, while the equivalent Born-Markov master equation current falls considerably (as

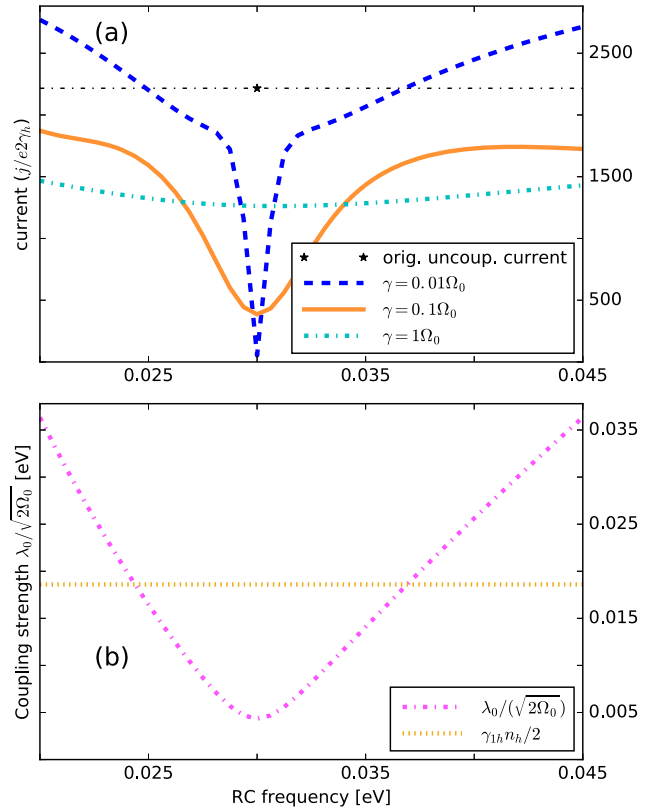


FIG. 4. (a) Current as a function of RC frequency  $\Omega_0$  (eV), where the transition rate  $\gamma_x$  is fixed so that the coupling strength  $\lambda_0$  increases as  $\Omega_0$  is moved off resonance. Both the default spectral density parameter  $\gamma = 0.1\Omega_0$  and the sharper one  $\gamma = 0.01\Omega_0$  lead to a sharp dip in current around resonance, the onset of which occurs around  $\lambda_0/\sqrt{2\Omega_0} \approx \gamma_{1h}n_h/2$ , whereas the broader one  $\gamma = \Omega_0$  is much flatter and exhibits no dip. (b) The behavior of the coupling strength  $\lambda_0/\sqrt{2\Omega_0}$  (dot-dashed pink curve) for  $\gamma = 0.1\Omega_0$  illustrates that the onset of the dip in the current does occur around  $\lambda_0/\sqrt{2\Omega_0} \approx \gamma_{1h}n_h/2$  (dashed orange curve).

it follows the correspondingly slower transition rate  $\gamma_x$ ). This suggests that it is predominantly the coupling strength itself, not the width of the spectral density, that increases the current in the Zeno-regime. As the coupling strength is increased so that we leave the Zeno regime, the width of the spectral density begins to have a larger influence, as per Fig. 4.

## B. Weak photon illumination regime and the Markov limit

The assumption of a very-high photon temperature, employed in many earlier studies on this heat-engine model,<sup>20–22,30,34</sup> maximizes the Carnot efficiency, and, in the classical model, maximizes the current. However it does not occur in natural or artificial photosynthetic systems, or photocells.<sup>66</sup> In addition, as we showed in Sec. IV A, it can lead to suppressed current flow due to dephasing. In Ref. 67, the authors consider the case of low-temperature illumination of a similar photosynthetic reaction center heat engine, corresponding to an maximal concentrated natural sunlight temperature of 6000 K, and hence a thermal occupation of  $n_h = 0.03$ , while also including the influence of non-degenerate dimer energies. In such conditions, they still found an advantage to the mechanism of including dimer-dimer couplings and subsequent bright to dark state conversion. Here, we can also

consider the influence of the RC mode at lower illumination levels and slower donor-acceptor transfer rate  $\gamma_c$  (larger values of  $\gamma_c$  were found to give a reduction in the current enhancement, relative to the uncoupled dimer example, in Ref. 67). This also allows us to finally answer the question of what happens in the weak phonon-coupling and Markov limit.

In Fig. 5(a), we observe that simultaneously lowering the temperature of the photon bath, donor-acceptor transfer rate  $\gamma_c$ , and the phonon coupling strength  $\lambda$ , and choosing a broad phonon spectral density, restores the Born-Markov limit such that all baths become additive, and all three models begin

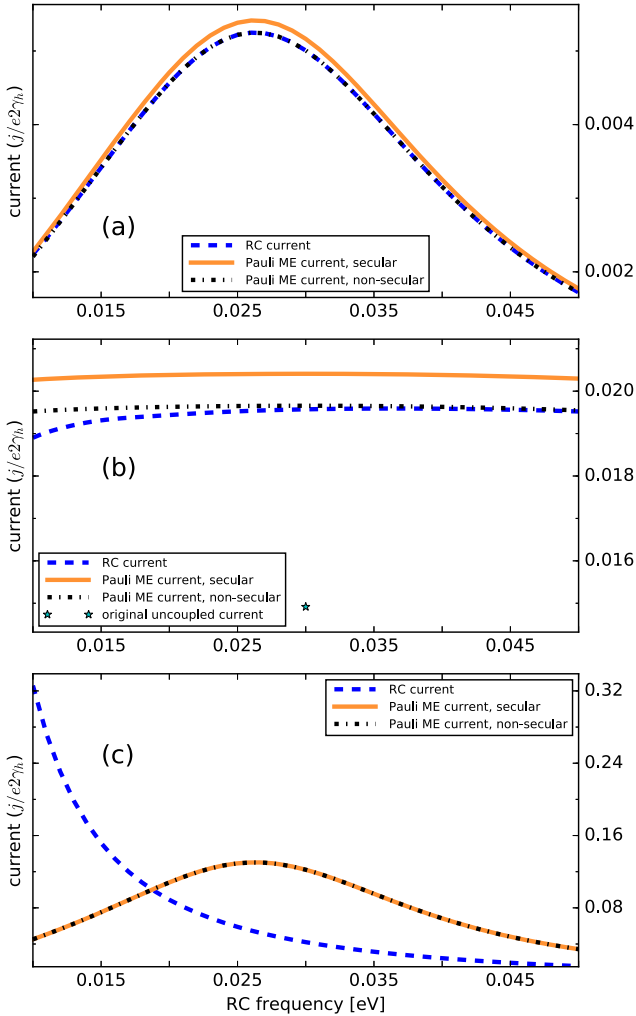


FIG. 5. (a) Current as a function of RC frequency (eV) for a fixed weak coupling strength  $\lambda_0 = 1.06 \times 10^{-5} \text{ eV}^{3/2}$ , with a correspondingly reduced photon temperature such that  $n_h = 0.03$ , and reduced donor-acceptor rate  $\gamma_c = 1 \times 10^{-6}$ , and for a broad phonon bath  $\gamma = \Omega_0$ . In this limit, we see that the non-secular master equation and the RC model predict the same current, suggesting the phonon environment is in a weak-coupling Markov limit, and that all environments are additive. (b) For the same low photon intensity  $n_h = 0.03$ , and donor-acceptor rate  $\gamma_c = 1 \times 10^{-6}$ , we see that increasing the phonon-emission rate back to  $\gamma_x = 25 \text{ meV}$ , by raising the phonon coupling to  $\lambda_0 = 1.06 \times 10^{-3} \text{ eV}^{3/2}$ , and choosing  $\gamma = 0.1\Omega_0$ , leads to a larger current, which can surpass that given by uncoupled dimers for equivalent parameters. We also see that the Markov models tend to overestimate the current. (c) When the phonon environment is in the weak-coupling-Markov limit ( $\lambda_0 = 1.06 \times 10^{-6} \text{ eV}^{3/2}$ ,  $\gamma = \Omega_0$ ), but the photon temperature is large  $n_h = 60000$  and the donor-acceptor rate is large  $\gamma_c = 6 \times 10^{-3}$ , we see again that the baths become non-additive, even when each individual bath could be considered to be in the Born-Markov limit.

to coincide (RC, secular, and non-secular master equations). Raising the phonon-coupling, and choosing  $\gamma$  so that the effective rate  $\gamma_x = 25 \text{ meV}$ , as in Sec. IV A, we see in Fig. 5(b) that the current again increases and exceeds the uncoupled dimer model current. The dependence on resonance now is very weak because of the bottleneck from the other rates. In this case, the Born-Markov master equations tend to overestimate the current, and the full RC model predicts a slightly smaller current than expected.

If we directly increase the coupling strength between the dimer and RC on resonance, Fig. 6(a), we eventually see diminishing returns in the RC model, with the current decreasing at a rate proportional to  $\lambda_0^2$  as we enter a regime where  $\lambda_0 > 10^{-3} \text{ eV}^{3/2}$ . This is at first glance counter-intuitive; however, if we consider that the time scales of the excited states of the dimer interacting with the RC are much faster than the other rates in the model, we notice that the thermal state of the dimer and RC subspace begins to dominate the behavior (the excited states and the RC thermalize before a donor-acceptor

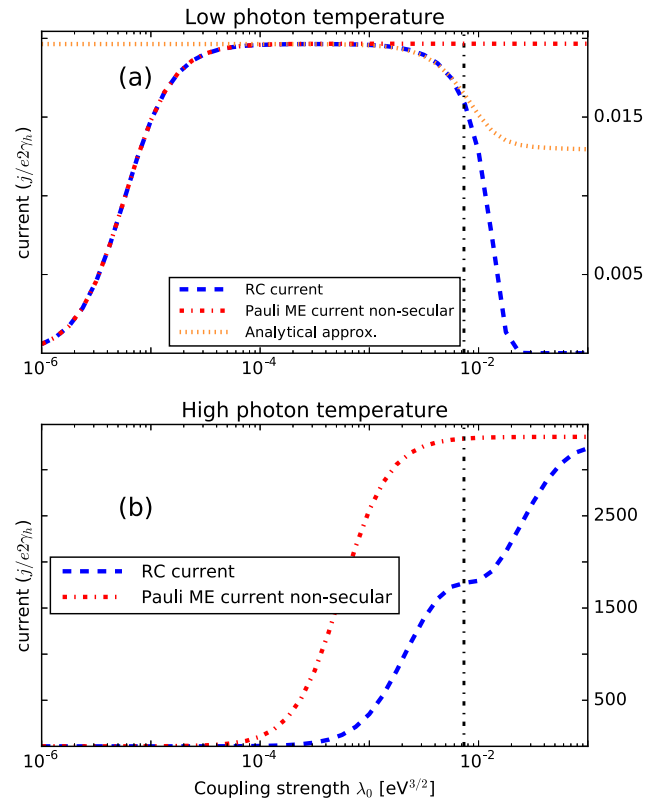


FIG. 6. Current as a function of coupling strength  $\lambda_0$  with the RC on resonance  $\Omega_0 = 2J$ . (a) is for the low-photon temperature such that  $n_h = 0.03$ , and reduced donor-acceptor rate  $\gamma_c = 1 \times 10^{-6}$ , and for  $\gamma = 0.1\Omega_0$ . Both the Pauli master equation and the RC model predict an optimal current around  $\lambda = 10^{-3} \text{ eV}^{3/2}$  because the current is limited by the weak photon illumination rate and donor-acceptor rate. For strong couplings, the Pauli master equation over-estimates the current because in the full RC model the strong interaction with the phonons reduces the matrix-elements which lead to current flow (see the main text). The orange dotted curve shows an approximate expression explaining the quadratic dependence of the current on the coupling strength. (b) shows the current dependence on coupling for the high-temperature limit  $n_h = 60000$  and fast donor-acceptor rate  $\gamma_c = 6 \times 10^{-3}$ . As in earlier figures, we see that the RC current is suppressed with respect to the Pauli master equation due to the effects described in the main text. The RC model predicts an inflection as the coupling strength becomes comparable with the resonance frequency (the line  $\lambda_0 = \Omega_0^{3/2}\sqrt{2}$  is plotted as a dashed vertical line).

transition can occur). In that case, the transition to the acceptor state  $\alpha$  will follow the transition matrix elements of the eigenstates of the dimer and RC subspace, weighted by their thermal populations. At 300 K, this is dominated by the first three excited states of the subspace. We can express these states perturbatively in the renormalized coupling strength  $\chi = \lambda_0/(\sqrt{2}\Omega_0^{3/2})$ , which, for example, for the ground state, gives, when  $\Omega_0 = 2J$ ,

$$|G\rangle = \left(1 - \frac{\chi^2}{8}\right)|x_2, 0\rangle - \frac{\chi}{2}|x_1, 1\rangle + \frac{\chi^2}{2\sqrt{2}}|x_2, 2\rangle. \quad (22)$$

The matrix elements connecting these states to the acceptor arise through the  $|x_2, n\rangle$  contributions. Interestingly, some of these contributions, like the reduction in probability of being in the  $|x_2, 0\rangle$  part of the ground state, arise due to the counter-rotating terms in the interaction with the phonons and leads to a corresponding reduction in the current proportional to  $1 - \frac{\chi^2}{4}$ . Summing up such matrix elements for all eigenstates of the dimer-RC subspace, and weighting them by their thermal occupations, provides a way to check the validity of this assumption, with an approximate expression for the current

$$\begin{aligned} \bar{j}(\chi)/2e\gamma_h \approx \max_{\chi} [j(\chi)/2e\gamma_h] \\ \times \sum_k P_k \left( \sum_n |\langle x_2, n | \psi_k \rangle|^2 \right) / \mathcal{N}. \quad (23) \end{aligned}$$

The eigenstates  $\psi_k$  are calculated numerically for the reduced model of the dimer excited states and RC from the Hamiltonian  $H'_S$ , which is  $H'_S$  projected onto the subspace containing just the dimer states  $x_1, x_2$ , and the RC states. The thermal occupation probabilities  $P_k$  are calculated from the thermal distribution  $\rho = \exp(-H'_S/k_B T)/Z$ , where  $Z = \text{Tr}[\exp(-H'_S/k_B T)]$ . The normalization of  $\bar{j}(\chi)$  by  $\mathcal{N}$  is chosen so that in the limit  $\chi \rightarrow 0$ ,  $\sum_k P_k \left( \sum_n |\langle x_2, n | \psi_k \rangle|^2 \right) / \mathcal{N} = 1$ . This approximate current is plotted in Fig. 6(a) and agrees well with the full numerical current of the RC model for  $\lambda_0$  in the range of applicability (an explicit second-order perturbative expansion also fits well for a smaller range of  $\chi$ , but we do not explicitly show it here because it is unwieldy). The approximate expression and the full numerics exhibit deviations for large  $\chi$  (and of course for very small  $\chi$ , where the current actually falls to zero, as there are no transitions to  $|x_2\rangle$  states at all in this limit).

Finally, in Fig. 5(c), we again set the phonon-bath parameters to be the same as Fig. 5(a) but raise  $\gamma_c$  and the photon temperature back to their values used in Sec. IV A. As in Sec. IV A, we again see a large discrepancy in the current, with a suppressed value for the RC model; this suggests that the issue of non-additive baths is more general than highly “non-Markovian” regimes, as is often assumed. The transition from Zeno to non-Zeno behavior, as a function of photon-bath temperature, occurs around the criteria given in Eq. (21).

## V. CONCLUSION

In this work, we analyzed the influence of a non-Markovian phonon bath on the efficiency of light harvesting in a photosynthetic reaction center considered as a quantum heat engine. Inspired by earlier studies, which found an advantage in breaking detailed balance by inducing energetic splitting between bright and dark states, we modeled the

phonon-mediated population transfer process from bright to dark states with the reaction coordinate formalism. This formalism allows us to model the influence of phonons for a wide range of coupling strengths and bath memory times.

We found that, counter-intuitively, bright photon illumination can suppress the current in the heat engine due to quantum Zeno-like dephasing of the exciton-phonon interaction. This suppression can be avoided by tuning properties of the phonon bath, and in doing so one can even generate currents significantly larger than the equivalent Markovian model. In the low photon temperature limit, by contrast, increasing the coupling to the phonon environment tends to reduce the current. Our results suggest that non-Markovian environments can be used to enhance the efficiency of light-harvesting systems but that the properties of the environment must be chosen, or designed, in artificial systems, carefully, as their influence can also be detrimental, in certain situations.

In addition, our results suggest that care must be taken whenever one considers multiple environments coupled to a single system, particularly when those environments induce dynamics on very different time scales,<sup>54</sup> even when one is apparently in a weak-coupling Markov limit for all baths.<sup>55</sup> This is a potentially useful observation, as it suggests that dissipative processes due to many commonly encountered perturbative environments, particularly in the solid state, might be modified by external environments.

Interestingly, it has recently become possible to program and implement Hamiltonian models of light harvesting in “quantum simulators,” as recently achieved with superconducting qubits,<sup>68,69</sup> ion traps,<sup>70</sup> and a NMR system.<sup>71</sup> In the case of superconducting qubits, dephasing noise of arbitrary spectral properties can be applied to each individual “chromophore” and their quantum coupling to photons can also be tuned in strength and frequency, allowing, in principle, a precise experimental test of non-additive environmental effects in both Markovian and non-Markovian photosynthetic energy transport. Further avenues for future study include the influence of coexisting underdamped and overdamped structured environments<sup>27–36,44</sup> in dimer photocells and how off-resonant dimers may alter the effects we discuss herein.<sup>67</sup>

## ACKNOWLEDGMENTS

We would like to thank Professor Matthias Troyer for creating the opportunity for this collaboration and Ahsan Nazir, Henry Maguire, and Mauro Cirio for helpful discussions and feedback on this work. M.W. has been fully supported by the RIKEN IPA program. N.L. and F.N. acknowledge support from the RIKEN-AIST Joint Research Fund and the Sir John Templeton Foundation. F.N. is also supported by the MURI Center for Dynamic Magneto-Optics via the Air Force Office of Scientific Research (AFOSR) (Grant No. FA9550-14-1-0040), Army Research Office (ARO) (Grant No. 73315PH), the Asian Office of Aerospace Research and Development (AOARD) (Grant No. FA2386-18-1-4045), Japan Science and Technology Agency (JST) (the ImPACT program and CREST Grant No. JPMJCR1676), and the Japan Society for the Promotion of Science (JSPS) (JSPS-RFBR Grant No. 17-52-50023).

## APPENDIX: BORN-MARKOV MASTER EQUATIONS

In Sec. IV, we compare results from the reaction coordinate master equation, Eq. (12), with two Markovian master equations which treat the interaction with the phonon environment under a standard Born-Markov assumption, i.e., as a rate  $\gamma_x$  driving transitions between the bright and dark states of the system. The secular version of this master equation is explicitly defined, using the same notation as in the main text, as

$$\begin{aligned} \dot{\rho}(t) = & -i[H_S, \rho(t)] \\ & + \mathcal{L}_{x_1b}[\rho(t)] + \mathcal{L}_{bx_1}[\rho(t)] \\ & + \mathcal{L}_{x_2x_1}[\rho(t)] + \mathcal{L}_{x_1x_2}[\rho(t)] \\ & + \mathcal{L}_{\alpha x_2}[\rho(t)] + \mathcal{L}_{x_2\alpha}[\rho(t)] \\ & + \mathcal{L}_{\beta b}[\rho(t)] + \mathcal{L}_{b\beta}[\rho(t)] \\ & + \mathcal{L}_{\alpha\beta}[\rho(t)] + \mathcal{L}_{\alpha b}[\rho(t)]. \end{aligned} \quad (\text{A1})$$

Now, all transitions are given by Lindblad generators  $\mathcal{L}_{AB} = [C_{AB}\rho(t)C_{AB}^\dagger - \frac{1}{2}\{C_{AB}^\dagger C_{AB}, \rho(t)\}]$ . In addition to the parameters  $C_{AB}$  defined in Eq. (19), we also have

$$\begin{aligned} C_{x_1b} &= \sqrt{2\gamma_h n_h}|x_1\rangle\langle b|, \\ C_{bx_1} &= \sqrt{2\gamma_h(1+n_h)}|b\rangle\langle x_1|, \\ C_{x_2x_1} &= \sqrt{\gamma_x(n_x+1)}|x_2\rangle\langle x_1|, \\ C_{x_1x_2} &= \sqrt{\gamma_x n_x}|x_1\rangle\langle x_2|, \\ C_{\alpha x_2} &= \sqrt{2\gamma_c(n_c+1)}|\alpha\rangle\langle x_2|, \\ C_{x_2\alpha} &= \sqrt{2\gamma_c n_c}|x_2\rangle\langle \alpha|. \end{aligned} \quad (\text{A2})$$

The factors of 2 in the photon baths and the transitions to the state  $|\alpha\rangle$  arise from the collective dipole coupling such that the matrix elements for these transitions are enhanced over those in the bare  $|a_1\rangle$  and  $|a_2\rangle$  basis.

Even in this case of a Markovian treatment of the phonon environment, the above equation is incomplete when the rates approach the coupling between the dimers,  $2J$ . In this case, one must treat transitions involving the excited states of the dimer with a non-Secular Born-Markov master equation. The equation of motion then becomes

$$\begin{aligned} \dot{\rho}(t) = & -i[H_S, \rho(t)] + \mathcal{M}_s[\rho(t)] + \mathcal{M}_{Q_h}[\rho(t)] \\ & + \mathcal{M}_{Q_c^{(\omega)}}[\rho(t)] + \mathcal{L}_{\beta b}[\rho(t)] + \mathcal{L}_{b\beta}[\rho(t)] \\ & + \mathcal{L}_{\alpha\beta}[\rho(t)] + \mathcal{L}_{\alpha b}[\rho(t)]. \end{aligned} \quad (\text{A3})$$

Again, the transitions not involving the excited dimer states are given by secular Born-Markov Lindblad generators. The transitions involving the hot photon bath, and those involving the electron transfer process to  $|\alpha\rangle$ , are given by the non-secular generator Eq. (14) (although now the eigenstates of the system do not include the RC mode). The Markovian phonon transitions are also given by Eq. (14) but with operator  $s = (|a_1\rangle\langle a_1| - |a_2\rangle\langle a_2|)$  and spectral density  $J_s(\omega) = J_0(\omega)$ , as per Eq. (6).

<sup>1</sup>G. S. Engel, T. R. Calhoun, E. L. Read, T.-K. Ahn, T. Mančal, Y.-C. Cheng, R. E. Blankenship, and G. R. Fleming, "Evidence for wavelike energy transfer through quantum coherence in photosynthetic systems," *Nature* **446**, 782 (2007).

<sup>2</sup>A. Ishizaki and G. R. Fleming, "Theoretical examination of quantum coherence in a photosynthetic system at physiological temperature," *Proc. Natl. Acad. Sci. U. S. A.* **106**, 17255–17260 (2009).

- <sup>3</sup>E. Collini, C. Y. Wong, K. E. Wilk, P. M. G. Curmi, P. Brumer, and G. D. Scholes, "Coherently wired light-harvesting in photosynthetic marine algae at ambient temperature," *Nature* **463**, 644 (2010).
- <sup>4</sup>Y.-C. Cheng and G. R. Fleming, "Dynamics of light harvesting in photosynthesis," *Annu. Rev. Phys. Chem.* **60**, 241–262 (2009).
- <sup>5</sup>A. Ishizaki and G. R. Fleming, "Quantum coherence in photosynthetic light harvesting," *Annu. Rev. Condens. Matter Phys.* **3**, 333–361 (2012).
- <sup>6</sup>N. Lambert, Y. N. Chen, Y. C. Cheng, C. M. Li, G. Y. Chen, and F. Nori, "Quantum biology," *Nat. Phys.* **9**, 10–18 (2013).
- <sup>7</sup>G. D. Scholes, G. R. Fleming, L. X. Chen, A. Aspuru-Guzik, A. Buchleitner, D. F. Coker, G. S. Engel, R. van Grondelle, A. Ishizaki, D. M. Jonas, J. S. Lundeen, J. K. McCusker, S. Mukamel, J. P. Ogilvie, A. Olaya-Castro, M. A. Ratner, F. C. Spano, K. B. Whaley, and X. Zhu, "Using coherence to enhance function in chemical and biophysical systems," *Nature* **543**, 647–656 (2017).
- <sup>8</sup>M. B. Plenio and S. F. Huelga, "Dephasing-assisted transport: Quantum networks and biomolecules," *New J. Phys.* **10**, 113019 (2008).
- <sup>9</sup>P. Rebentrost, M. Mohseni, I. Kassal, S. Lloyd, and A. Aspuru-Guzik, "Environment-assisted quantum transport," *New J. Phys.* **11**, 33003 (2009).
- <sup>10</sup>F. Caruso, A. W. Chin, A. Datta, S. F. Huelga, and M. B. Plenio, "Highly efficient energy excitation transfer in light-harvesting complexes: The fundamental role of noise-assisted transport," *J. Chem. Phys.* **131**, 105106 (2009).
- <sup>11</sup>A. W. Chin, A. Datta, F. Caruso, M. B. Plenio, and S. F. Huelga, "Noise-assisted energy transfer in quantum networks and light-harvesting complexes," *New J. Phys.* **12**, 065002 (2010).
- <sup>12</sup>F. Caycedo-Soler, F. J. Rodriguez, L. Quiroga, and N. F. Johnson, "Light-harvesting mechanism of bacteria exploits a critical interplay between the dynamics of transport and trapping," *Phys. Rev. Lett.* **104**, 158302 (2010).
- <sup>13</sup>A. W. Chin, J. Prior, R. Rosenbach, F. Caycedo-Soler, S. F. Huelga, and M. B. Plenio, "The role of non-equilibrium vibrational structures in electronic coherence and recoupling in pigment-protein complexes," *Nat. Phys.* **9**, 113–118 (2013).
- <sup>14</sup>C.-M. Li, N. Lambert, Y.-N. Chen, G.-Y. Chen, and F. Nori, "Witnessing quantum coherence: From solid-state to biological systems," *Sci. Rep.* **2**, 885 (2012); e-print [arXiv:1212.0194](https://arxiv.org/abs/1212.0194).
- <sup>15</sup>L. G. Mouroukh and F. Nori, "Energy transfer efficiency in the chromophore network strongly coupled to a vibrational mode," *Phys. Rev. E* **92**, 052720 (2015).
- <sup>16</sup>A. W. Chin, S. F. Huelga, and M. B. Plenio, "Coherence and decoherence in biological systems: Principles of noise assisted transport and the origin of long-lived coherences," *Philos. Trans. R. Soc., A* **370**, 3638 (2012); e-print [arXiv:1203.5072v1](https://arxiv.org/abs/1203.5072v1).
- <sup>17</sup>S. F. Huelga and M. B. Plenio, "Vibrations, quanta and biology," *Contemp. Phys.* **54**, 181 (2013); e-print [arXiv:1307.3530v1](https://arxiv.org/abs/1307.3530v1).
- <sup>18</sup>E. Romero, R. Augulis, V. I. Novoderezhkin, M. Ferretti, J. Thieme, D. Zigmantas, and R. Van Grondelle, "Quantum coherence in photosynthesis for efficient solar-energy conversion," *Nat. Phys.* **10**, 676 (2014).
- <sup>19</sup>F. D. Fuller, J. Pan, A. Gelzins, V. Butkus, S. S. Senlik, D. E. Wilcox, C. F. Yocum, L. Valkunas, D. Abramavicius, and J. P. Ogilvie, "Vibronic coherence in oxygenic photosynthesis," *Nat. Chem.* **6**, 706 (2014).
- <sup>20</sup>K. E. Dorfman, D. V. Voronine, S. Mukamel, and M. O. Scully, "Photo-synthetic reaction center as a quantum heat engine," *Proc. Natl. Acad. Sci. U. S. A.* **110**, 2746–2751 (2013).
- <sup>21</sup>C. Creatore, M. A. Parker, S. Emmott, and A. W. Chin, "Efficient biologically inspired photocell enhanced by delocalized quantum states," *Phys. Rev. Lett.* **111**, 253601 (2013).
- <sup>22</sup>Y. Zhang, S. Oh, F. H. Alharbi, G. S. Engel, and S. Kais, "Delocalized quantum states enhance photocell efficiency," *Phys. Chem. Chem. Phys.* **17**, 5743–5750 (2015).
- <sup>23</sup>W. Shockley and H. J. Queisser, "Detailed balance limit of efficiency of *p-n* junction solar cells," *J. Appl. Phys.* **32**, 510–519 (1961).
- <sup>24</sup>J.-L. Brédas, E. H. Sargent, and G. D. Scholes, "Photovoltaic concepts inspired by coherence effects in photosynthetic systems," *Nat. Mater.* **16**, 35 (2017).
- <sup>25</sup>V. Holubec and T. Novotný, "Effects of noise-induced coherence on the performance of quantum absorption refrigerators," *J. Low Temp. Phys.* **192**, 147–168 (2018).
- <sup>26</sup>K. D. B. Higgins, B. W. Lovett, and E. M. Gauger, "Quantum-enhanced capture of photons using optical ratchet states," *J. Phys. Chem. C* **121**, 20714–20719 (2017).
- <sup>27</sup>D. H. Santamore, N. Lambert, and F. Nori, "Vibrationally mediated transport in molecular transistors," *Phys. Rev. B* **87**, 075422 (2013); e-print [arXiv:1210.7098](https://arxiv.org/abs/1210.7098).

- <sup>28</sup>E. K. Irish, R. Gómez-Bombarelli, and B. W. Lovett, "Vibration-assisted resonance in photosynthetic excitation-energy transfer," *Phys. Rev. A* **90**, 012510 (2014).
- <sup>29</sup>E. J. O'Reilly and A. Olaya-Castro, "Non-classicality of the molecular vibrations assisting exciton energy transfer at room temperature," *Nat. Commun.* **5**, 3012 (2014).
- <sup>30</sup>N. Killoran, S. F. Huelga, and M. B. Plenio, "Enhancing light-harvesting power with coherent vibrational interactions: A quantum heat engine picture," *J. Chem. Phys.* **143**, 155102 (2015).
- <sup>31</sup>R. Stones and A. Olaya-Castro, "Vibronic coupling as a design principle to optimize photosynthetic energy transfer," *Chem* **1**, 822–824 (2016).
- <sup>32</sup>P. Strasberg, G. Schaller, N. Lambert, and T. Brandes, "Nonequilibrium thermodynamics in the strong coupling and non-Markovian regime based on a reaction coordinate mapping," *New J. Phys.* **18**, 073007 (2016).
- <sup>33</sup>E. K. Levi, E. K. Irish, and B. W. Lovett, "Coherent exciton dynamics in a dissipative environment maintained by an off-resonant vibrational mode," *Phys. Rev. A* **93**, 042109 (2016).
- <sup>34</sup>H.-B. Chen, P.-Y. Chiu, and Y.-N. Chen, "Vibration-induced coherence enhancement of the performance of a biological quantum heat engine," *Phys. Rev. E* **94**, 052101 (2016).
- <sup>35</sup>D. Newman, F. Mintert, and A. Nazir, "Performance of a quantum heat engine at strong reservoir coupling," *Phys. Rev. E* **95**, 032139 (2017).
- <sup>36</sup>M. Qin, H. Z. Shen, X. L. Zhao, and X. X. Yi, "Effects of system-bath coupling on a photosynthetic heat engine: A polaron master-equation approach," *Phys. Rev. A* **96**, 012125 (2017).
- <sup>37</sup>I. de Vega and D. Alonso, "Dynamics of non-Markovian open quantum systems," *Rev. Mod. Phys.* **89**, 015001 (2017).
- <sup>38</sup>H.-B. Chen, N. Lambert, Y.-C. Cheng, Y.-N. Chen, and F. Nori, "Using non-Markovian measures to evaluate quantum master equations for photosynthesis," *Sci. Rep.* **5**, 12753 (2015); e-print [arXiv:1503.02412v1](https://arxiv.org/abs/1503.02412v1).
- <sup>39</sup>A. Fruchtmann, N. Lambert, and E. M. Gauger, "When do perturbative approaches accurately capture the dynamics of complex quantum systems?," *Sci. Rep.* **6**, 28204 (2016); e-print [arXiv:1512.09086](https://arxiv.org/abs/1512.09086).
- <sup>40</sup>Y. Tanimura and R. Kubo, "Time evolution of a quantum system in contact with a nearly Gaussian-Markoffian noise bath," *J. Phys. Soc. Jpn.* **58**, 101–114 (1989).
- <sup>41</sup>C. Kreisbeck and T. Kramer, "Long-lived electronic coherence in dissipative exciton dynamics of light-harvesting complexes," *J. Phys. Chem. Lett.* **3**, 2828–2833 (2012); e-print [arXiv:1203.1485](https://arxiv.org/abs/1203.1485).
- <sup>42</sup>A. Garg, J. N. Onuchic, and V. Ambegaokar, "Effect of friction on electron transfer in biomolecules," *J. Chem. Phys.* **83**, 4491–4503 (1985).
- <sup>43</sup>J. Iles-Smith, N. Lambert, and A. Nazir, "Environmental dynamics, correlations, and the emergence of noncanonical equilibrium states in open quantum systems," *Phys. Rev. A* **90**, 032114 (2014).
- <sup>44</sup>J. Iles-Smith, A. G. Dijkstra, N. Lambert, and A. Nazir, "Energy transfer in structured and unstructured environments: Master equations beyond the Born-Markov approximations," *J. Chem. Phys.* **144**, 044110 (2016).
- <sup>45</sup>N. Makri, "Quantum dissipative dynamics: A numerically exact methodology," *J. Phys. Chem. A* **102**, 4414–4427 (1998).
- <sup>46</sup>P. Nalbach, A. Ishizaki, G. R. Fleming, and M. Thorwart, "Iterative path-integral algorithm versus cumulant time-nonlocal master equation approach for dissipative biomolecular exciton transport," *New J. Phys.* **13**, 063040 (2011).
- <sup>47</sup>U. Manthe, "A multilayer multiconfigurational time-dependent hartree approach for quantum dynamics on general potential energy surfaces," *J. Chem. Phys.* **128**, 164116 (2008).
- <sup>48</sup>J. Schulze and O. Kuhn, "Explicit correlated exciton-vibrational dynamics of the FMO complex," *J. Phys. Chem. B* **119**, 6211–6216 (2015).
- <sup>49</sup>A. Chin, J. Prior, R. Rosenbach, F. Caycedo-Soler, S. Huelga, and M. Plenio, "The role of non-equilibrium vibrational structures in electronic coherence and recoherence in pigment-protein complexes," *Nat. Phys.* **9**, 113 (2013).
- <sup>50</sup>J. Prior, I. de Vega, A. W. Chin, S. F. Huelga, and M. B. Plenio, "Quantum dynamics in photonic crystals," *Phys. Rev. A* **87**, 013428 (2013).
- <sup>51</sup>F. A. Y. N. Schröder, D. H. P. Turban, A. J. Musser, N. D. M. Hine, and A. W. Chin, "Multi-dimensional tensor network simulation of open quantum dynamics in singlet fission," preprint [arXiv:1710.01362](https://arxiv.org/abs/1710.01362) (2017).
- <sup>52</sup>Y. Fujihashi, L. Chen, A. Ishizaki, J. Wang, and Y. Zhao, "Effect of high-frequency modes on singlet fission dynamics," *J. Chem. Phys.* **146**, 044101 (2017).
- <sup>53</sup>R. Stones, H. Hossein-Nejad, R. van Grondelle, and A. Olaya-Castro, "On the performance of a photosystem II reaction centre-based photocell," *Chem. Sci.* **8**, 6871 (2017).
- <sup>54</sup>G. G. Giusteri, F. Recrosi, G. Schaller, and G. L. Celardo, "Interplay of different environments in open quantum systems: Breakdown of the additive approximation," *Phys. Rev. E* **96**, 012113 (2017).
- <sup>55</sup>M. T. Mitchison and M. B. Plenio, "Non-additive dissipation in open quantum networks out of equilibrium," *New J. Phys.* **20**, 033005 (2018).
- <sup>56</sup>D. Gruss, A. Smolyanitsky, and M. Zwolak, "Communication: Relaxation-limited electronic currents in extended reservoir simulations," *J. Chem. Phys.* **147**, 141102 (2017).
- <sup>57</sup>P. K. Ghosh, A. Y. Smirnov, and F. Nori, "Modeling light-driven proton pumps in artificial photosynthetic reaction centers," *J. Chem. Phys.* **131**, 035102 (2009); e-print [arXiv:0901.2170v2](https://arxiv.org/abs/0901.2170v2).
- <sup>58</sup>W. T. Pollard and R. A. Friesner, "Solution of the Redfield equation for the dissipative quantum dynamics of multilevel systems," *J. Chem. Phys.* **100**, 5054 (1994).
- <sup>59</sup>R. Martinazzo, B. Vacchini, K. H. Hughes, and I. Burghardt, "Communication: Universal Markovian reduction of Brownian particle dynamics," *J. Chem. Phys.* **134**, 011101 (2011).
- <sup>60</sup>A. Dodin, T. V. Tscherbul, and P. Brumer, "Quantum dynamics of incoherently driven V-type systems: Analytic solutions beyond the secular approximation," *J. Chem. Phys.* **144**, 244108 (2016).
- <sup>61</sup>M. Wendling, T. Pullerits, M. A. Przyjalowski, S. I. E. Vulto, T. J. Aartsma, R. van Grondelle, and H. van Amerongen, "Electron-vibrational coupling in the Fenna-Matthews-Olson complex of *Prosthecochloris aestuarii* determined by temperature-dependent absorption and fluorescence line-narrowing measurements," *J. Phys. Chem. B* **104**, 5825–5831 (2000).
- <sup>62</sup>J. R. Johansson, P. D. Nation, and F. Nori, "QuTiP: An open-source python framework for the dynamics of open quantum systems," *Comput. Phys. Commun.* **183**, 1760 (2012).
- <sup>63</sup>J. R. Johansson, P. D. Nation, and F. Nori, "QuTiP 2: A python framework for the dynamics of open quantum systems," *Comput. Phys. Commun.* **184**, 1234–1240 (2013).
- <sup>64</sup>H.-P. Breuer and F. Petruccione, *The Theory of Open Quantum Systems* (Oxford University Press, 2002).
- <sup>65</sup>S. Ashhab, J. R. Johansson, A. M. Zagorskin, and F. Nori, "Single-artificial-atom lasing using a voltage-biased superconducting charge qubit," *New J. Phys.* **11**, 023030 (2009).
- <sup>66</sup>S. Oh, "How much is the efficiency of solar cells enhanced by quantum coherence?," e-print [arXiv:1709.08337](https://arxiv.org/abs/1709.08337) (2017).
- <sup>67</sup>A. Fruchtmann, R. Gómez-Bombarelli, B. W. Lovett, and E. M. Gauger, "Photocell optimization using dark state protection," *Phys. Rev. Lett.* **117**, 203603 (2016).
- <sup>68</sup>A. Potocnik, A. Bargerbos, F. A. Y. N. Schröder, S. A. Khan, M. C. Collodo, S. Gasparinetti, Y. Salathe, C. Creatore, C. Eichler, H. E. Törcü, A. W. Chin, and A. Wallraff, "Studying light-harvesting models with superconducting circuits," *Nat. Commun.* **9**, 904 (2018).
- <sup>69</sup>A. Chin, E. Manguad, O. Atabek, and M. Desouter-Lecomte, "Coherent quantum dynamics launched by incoherent relaxation in a quantum circuit simulator of a light-harvesting complex," *Phys. Rev. A* **97**, 063823 (2018).
- <sup>70</sup>D. J. Gorman, B. Hemmerling, E. Megidish, S. A. Moeller, P. Schindler, M. Sarovar, and H. Haeflner, "Engineering vibrationally assisted energy transfer in a trapped-ion quantum simulator," *Phys. Rev. X* **8**, 011038 (2018).
- <sup>71</sup>B.-X. Wang, M.-J. Tao, Q. Ai, T. Xin, N. Lambert, D. Ruan, Y.-C. Cheng, F. Nori, F.-G. Deng, and G.-L. Long, "Quantum simulation of photosynthetic energy transfer," e-print [arXiv:1801.09475](https://arxiv.org/abs/1801.09475) (2018).